Comparing Hall Sensor-based Commutation and Current-Controlled Field-Oriented Control Strategies for BLDC Motors with Application in Electric Scooter

Sajad Solgi*, Andreas Stadler, Kazem Pourhossein, Detlef Schulz
Chair of Electrical Power Systems
Helmut Schmidt University / University of the Federal Armed Forces Hamburg
Hamburg, Germany
*solgis@hsu.hamburg

***Abstract* – This paper investigates the influence of two different control methods on the performance of Brushless DC (BLDC) motors using MATLAB/Simulink. BLDC motors are widely used in industrial and consumer applications due to their high efficiency, reliability, and compactness. The performance of this motor is significantly affected by the choice of control strategy used for inverter control. This study compares Current-Controlled Field-Oriented Control (CC-FOC) and Hall Sensor-based Commutation (HSC) in terms of torque ripple and speed response. Both methods are simulated on a 350W BLDC motor used in an electric scooter (e-scooter). Simulation models are developed in MATLAB/Simulink to evaluate each technique under identical operating conditions. The findings show that the CC-FOC method has a significantly higher response capability at maximum speeds, reduces torque ripples and improves the dynamic stability of the system compared to the HSC method. The results provide insights into the trade-offs between control complexity and motor performance, offering guidance for selecting appropriate control strategy in practical applications.**

Keywords – BLDC Motor, Current-Controlled Field-Oriented Control (CC-FOC), Hall Sensor-based Commutation (HSC), Torque Ripple, Speed Control

NOMENCLATUR

back-EMF	Back electromotive force
BLDC	Brushless DC
CC-FOC	Current-Controlled Field-Oriented Control
d-axis	Direct–axis
DTC	Direct torque control
e-scooter	Electric scooter
HCC	Hysteresis current control
PI	Proportional–integral
PID	Proportional–integral–derivative
PMBLDC	Permanent magnet brushless DC
q-axis	Quadrature–axis
SPWM	Sinusoidal pulse width modulation
SVPWM	Space vector pulse width modulation

VARIABLES

$e_{\mathrm{a}}, e_{\mathrm{b}}, e_{\mathrm{c}}$	Phase back-EMFs
$i_{\mathrm{a}}, i_{\mathrm{b}}, i_{\mathrm{c}}$	Phase currents
$i_{\mathrm{d}}, i_{\mathrm{q}}, i_{0}$	Current along the d-axis, q-axis and zero component
k_{e}	Back-EMF constant
K_{i}	Integral coefficient
K_{p}	Proportional coefficient
k_{t}	Torque constant
L	Self-inductance
M	Mutual inductance
p	Number of poles
P_{e}	Electromagnetic power
R_{a} , R_{b}, R_{c}	Stator phase resistances
T_{e}	Electromagnetic torque
$v_{\mathrm{an}}, v_{\mathrm{bn}}, v_{\mathrm{cn}}$	Phase voltages
v_{d}, v_{q}, v_{0}	d-axis, q-axis and zero-sequence voltages
ω_{e}	Electrical rotation
ω_{m}	Mechanical rotation
θ	Electric field angle of the rotor

DOI: 10.24405/22063

I. INTRODUCTION

Permanent magnet BLDC motors are used in applications such as drones, electric vehicles, industrial fans, and precision instruments. The use of BLDC motors in electric vehicles such as electric scooters, electric bicycles and electric cars is increasing due to advantages such as high torque-to-weight ratio, high efficiency and low maintenance requirements [1]. Unlike conventional brushed motors, BLDC motors rely on electronic commutation, which makes the control strategy a critical factor in determining overall system performance. For this reason, choosing the right control method for these motors plays a decisive role in optimizing performance, increasing efficiency and improving the user experience in electric vehicles.

The rotor of PMBLDC motors contains permanent magnets, and their stator contains windings arranged in three phases. Their operating principles are such that at any given moment, two stator windings must be in the excited state (one with a positive voltage and the other one with a negative voltage) and the third phase remains in the suspended state (without excitation) [1]. A rotating magnetic field will be created in the air gap between stator and the rotor. The permanent magnets of the rotor are affected by this field and start to rotate.

Motor control is usually done by a three-phase inverter that energizes the appropriate winding according to the rotor position.

BLDC motor control systems may be sensor-based, such as Hall sensor control (HSC), or sensor less. In the first method, the rotor position and the speed are determined directly by motor speed and Hall sensors, but in the second method, the rotor position is estimated from measuring motor parameters such as back-EMF waveform. For instance, in [1], the rotor position and the speed are estimated by sensing the magnetic field of the internal permanent magnets of the BLDC motor, using two different multidimensional models based on the Fourier series. BLDC motor control systems can be based on either a scalar or vector systems. In scalar control method, which is based on a constant ratio of applied voltage to the frequency [2], since the flux and torque are not directly controlled, it's not suitable for high-precision applications [3]. In vector control - also known as field-oriented control (FOC) - the three-phase stator currents are transformed from a three-phase system into two orthogonal components [4] -the direct-axis (d-axis) and quadrature-axis (q-axis) components - using the Park and Clarke transformations. These components allow independent control of magnetic flux and torque. In addition to Current-Controlled Field-Oriented Control **(**CC-FOC), the modulation techniques like Space Vector Pulse Width Modulation (SVPWM) and Sinusoidal Pulse Width Modulation (SPWM) are commonly used in FOC to generate the switching signals for the inverter. Different PWM strategies can significantly influence the dynamic behavior, torque ripple, and energy efficiency of BLDC motors. The effect of SPWM and SVPWM on the performance of BLDC motor has been compared in [5].

Several control methods such as fault tolerance control, electromagnetic interference reduction, FOC, direct torque control (DTC), current shaping, input voltage control and drive-inverter topology reducing torque ripples, are introduced in [6]. The effect of different PWM schemes on common-mode noise (unwanted voltage that appears between the neutral point of BLDC motor phases and the ground) BLDC motor drives, focusing on noise reduction through modulation and filtering techniques, is investigated in [7-8]. In [9], a BLDC motor is modeled and after obtaining its transfer function, a proportional–integral–derivative (PID) controller is designed for its closed-loop model, whose input is the speed and current of the motor phases, and its output is the generation of signals for the inverter gates, and this controller operates based on hysteresis current control (HCC). Reference [10] presents FOC for precise rotor position and torque control of a BLDC motor. It describes the Park and inverse Park transformations and develops the motor model in the d–q reference frame along with the corresponding inverter model. Reference [11] provides a mathematical and geometric explanation of how electrical quantities are transformed between the abc, αβ0, and dq0 reference frames. It derives both the forward (Park) and inverse (inverse Park) transformation matrices, offering a unified geometric understanding of how these transformations simplify the machine analysis and control in rotating reference frames.

This paper aims to model and compare CC-FOC and HSC techniques using MATLAB/Simulink and analyze their impact on the performance of a 350 W BLDC motor. The goal is to provide comparative study that can aid engineers and researchers in selecting the most suitable control method for specific applications.

II. MODELING AND SIMULATION

The overall system model is shown in FIGURE 1. Signals received from hall effect sensors sent to the BLDC motor controller and finally this control applied via PWM signals to the bridge hardware. FIGURE 2 shows the 40 poles 350-W BLDC motor of an e-scooter. The three digital Hall sensors attached to the stator are supplied with a voltage of 5 volts, and as the rotor rotates, the signals change from 0 to 5 V and they send the information of the rotor positions to the control system. The reference signals of the three Hall sensors shown in FIGURE 3 must be generated according to Hall A, Hall B and Hall C waves. These sensors generate a total of six different states (001, 010, 011, 100, 101, 110). The corresponding three phase voltages in this figure show the generated voltage waves according to the rotor position. The three phase voltage waves in FIGURE 3 show that two phases are always supplied (one positive and the other one negative) simultaneously, and the third phase remains floating. That means that the motor constantly receives positive torque from two phases, and the motor always generates a uniform and positive torque. For example, in state 1, the motor generates positive torque from phases "U" and "V".

According to Kirchhoff's voltage law, the voltage applied to each phase of the motor is equal to sum of the voltage drop across the winding resistance and the rate of change of the flux linkage (induced voltage or Back-EMF). The BLDC motor equations are determined in (1) – (3)

$$v_{\mathrm{an}} = R_{\mathrm{a}} i_{\mathrm{a}} + (L - M)\frac{di_{\mathrm{a}}}{dt} + e_{\mathrm{a}} \tag{1}$$

$$v_{\mathrm{bn}} = R_{\mathrm{b}} i_{\mathrm{b}} + (L - M)\frac{di_{\mathrm{b}}}{dt} + e_{\mathrm{b}} \tag{2}$$

$$v_{\mathrm{cn}} = R_{\mathrm{c}} i_{\mathrm{c}} + (L - M)\frac{di_{\mathrm{c}}}{dt} + e_{\mathrm{c}} \tag{3}$$

where, R_{a} , R_{b} and R_{c} are the stator phase resistances, all of which are equal and are denoted by R. The phase currents are

i_a, i_b and i_c. The self-inductance is L, and the mutual inductance of the stator phases is M.

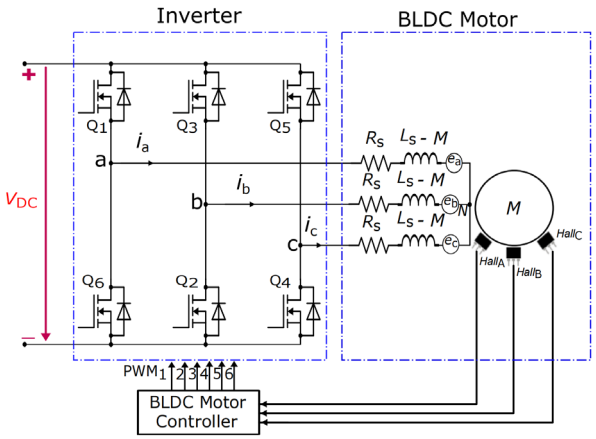

FIGURE 1:OVERALL SYSTEM MODEL.

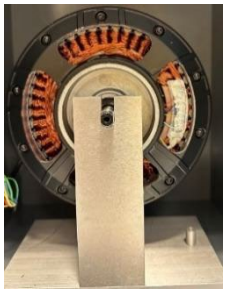

FIGURE 2:BLDC MOTOR FOR "SXT.SCOOTERS MAX".

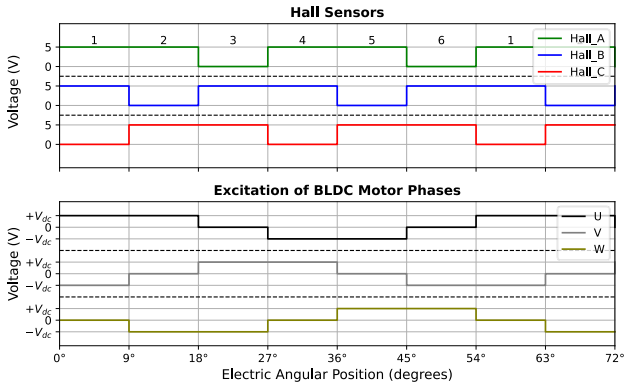

FIGURE 3:HALL SENSORS SIGNALS AND THE EXCITATION STRATEGY OF BLDC MOTOR PHASES.

The electrical rotation ω_e is defined in (4).

$$\omega_e = \frac{p}{2}\omega_m \tag{4}$$

where, ω_m is the mechanical rotation and p is the number of poles. The back-EMF is defined in (5).

$$e_a = k_e \omega_e \tag{5}$$

where, k_e is the back-EMF constant. The relationships between electromagnetic torque and current as well as the electrical rotation are obtained from (6) and (7).

$$T_e = k_t I \tag{6}$$

$$T_e = \frac{P_e}{\omega_e} \tag{7}$$

where, k_t is the torque constant, I is the stator phase current, and P_e is the electromagnetic power and it is obtained from (8).

$$P_e = e_a i_a + e_b i_b + e_c i_c \tag{8}$$

A. HSC Strategy

The control system based on HSC discussed in this paper is shown in FIGURE 4 [12]. In the Hall control system shown in FIGURE 4, the instantaneous motor speed $\omega_{m_{meas}}$ is compared to a reference speed $\omega_{m_{ref}}$ and from that the speed error signal e_ω is generated. This speed error signal is fed into a PI controller to produce a reference torque. At the moment of starting the motion (when $\omega_m = 0$), e_ω is high, so the controller produces the maximum possible torque. As the speed approaches the reference value, e_ω and its integral decrease, and subsequently the torque decreases. The maximum torque that the controller can apply, assuming no current or torque saturation, is:

$$T_{max} = K_p e_\omega + K_i \int e_\omega \, dt \tag{9}$$

here, the PI controller coefficients should be set in such a way that the maximum motor torque appears at its output. The controller's integral and proportional coefficient are set to $K_i = 1$ and $K_p = 20$, respectively. The maximum motor torque T_{max} is then compared with the instantaneous motor torque and produces the maximum torque error e_{Tmax}. By dividing it by the torque coefficient $k_t = 0.67$, the maximum current value I_{max} is produced. The produced maximum current value is then multiplied by the reference signals e_a, e_b, and e_c, produced from the decoder system generated from the input rotor position signals. The pattern of generating these signals from the decoder is based on TABLE I. In this table, $Hall_A$, $Hall_B$, and $Hall_C$ are the Hall sensor signals and Q1 - Q6 are the inverter switches. Hall sensors are used here to estimate the rotor position. The control system turns the appropriate phase on, according to the instantaneous rotor position. After multiplying the maximum current value I_{max} and the reference signals e_a, e_b, and e_c, produced from the decoder system, the reference current I_{ref} is generated. By comparing it with the actual measured phase current i_{meas}, the current error signal e_i is generated ($e_i = i_{ref} - i_{meas}$).

TABLE I: SWITCHING REFERENCE.

$Hall_A$	$Hall_A$	$Hall_A$	e_a	e_a	e_a	Q1	Q2	Q3	Q4	Q5	Q6
0	0	1	1	-1	+1	0	1	0	0	1	0
0	1	0	-1	+1	0	0	0	1	0	0	1
0	1	1	-1	0	+1	0	0	0	0	1	1
1	0	0	+1	0	-1	1	0	0	1	0	0
1	0	1	+1	-1	0	1	1	0	0	0	0
1	1	0	0	+1	-1	0	0	1	1	0	0

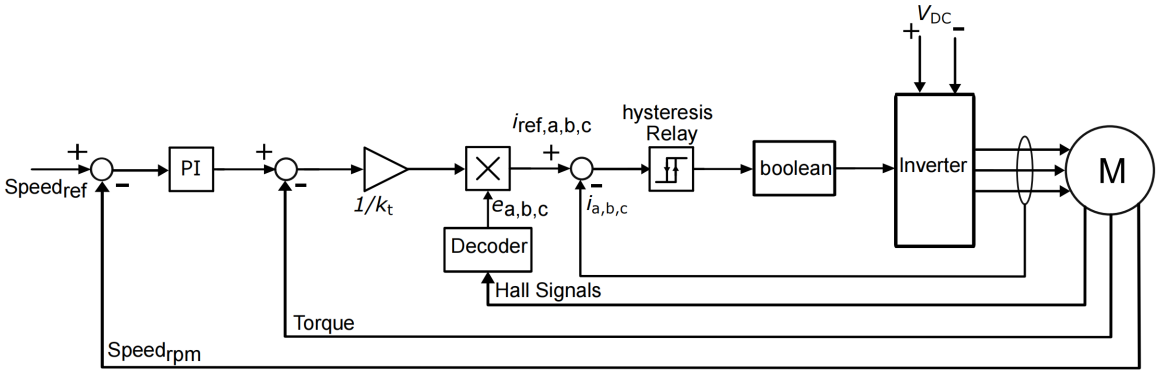

FIGURE 4:BLOCK DIAGRAM OF HSC-BASED CLOSED-LOOP SPEED AND TORQUE CONTROL FOR A BLDC MOTOR.

The output of this function enters a pulse generation logic circuit for the inverter switches by passing through a type of hysteresis relay (or deadband comparator) and then a boolean relay that has a boolean state (0 or 1).

The deadband comparator relay has two on and off thresholds:

- On threshold: while $e_{\mathrm{i}} > 0.1$
- Off threshold: while $e_{\mathrm{i}} < -0.1$

For $-0.1 \leq e_{\mathrm{i}}(t) \leq 0.1$, the previous value remains on the output, which means maintaining the current state in the dead band.

The three signals generated, are then applied to the inverter switches to apply power to the stator phases according to FIGURE 3.

B. CC-FOC Strategy

The control system based on CC-FOC discussed in this paper is shown in FIGURE 5. In this method, first the stator currents from a three-phase system are converted to d-q references in a rotating vector system. The torque component (i_{q}) and the magnetization component (i_{d}) are controlled independently. The current along the d-axis is i_{d} , which is in the same direction as the rotor magnetic field, and the current along the q-axis is i_{q}, which is perpendicular to the rotor magnetic field.

The overall direct conversion from three-phase current to d-q-0 (known as Park's Transformation) can be written as (10) [11].

$$\begin{bmatrix} i_{\mathrm{d}} \\ i_{\mathrm{q}} \\ i_0 \end{bmatrix} = \frac{2}{3}\begin{bmatrix} cos(\theta) & cos(\theta - 2\pi/3) & cos(\theta + 2\pi/3) \\ -sin(\theta) & -sin(\theta - 2\pi/3) & -sin(\theta + 2\pi/3) \\ \frac{1}{2} & \frac{1}{2} & \frac{1}{2} \end{bmatrix}\begin{bmatrix} i_{\mathrm{a}} \\ i_{\mathrm{b}} \\ i_{\mathrm{c}} \end{bmatrix} \quad (10)$$

The zero component i_0 in balanced three-phase systems is zero. θ is the electric field angle of the rotor, which is obtained from the integration of the electric angular velocity obtained from (11).

$$\theta = \int \omega_{\mathrm{e}} dt \quad (11)$$

In FOC, the $I_{\max}$ generated from the speed control loop is the q-axis reference current $I_{\mathrm{q,ref}}$. By comparing this current with i_{q}, the instantaneous q-axis current error e_{q} is generated. Since this motor has permanent magnets and the rotor magnetic field is uniform, the motor has a constant reluctance, and hence the d-axis reference current is set to 0. By comparing i_{d} with 0, the instantaneous d-axis current error e_{d} is produced. The error signals after passing through a PI controller with integral and proportional coefficients of $K_{\mathrm{id}} = K_{\mathrm{iq}} = 2000$ and $K_{\mathrm{pd}} = K_{\mathrm{pq}} = 40$, respectively, give the d-axis and q-axis voltages v_d, v_q as outputs, as defined in (12) and (13).

$$v_{\mathrm{d}} = K_{\mathrm{pd}} e_{\mathrm{d}} + K_{\mathrm{id}} \int e_{\mathrm{d}}\, dt \quad (12)$$

$$v_{\mathrm{q}} = K_{\mathrm{pq}} e_{\mathrm{q}} + K_{\mathrm{iq}} \int e_{\mathrm{q}}\, dt \quad (13)$$

After computing the control voltages in the rotating dq0 reference frame, these voltages must be transformed back to the stationary three-phase (abc) system. The inverse Park transformation is defined as shown in (14) [11].

$$\begin{bmatrix} v_{\mathrm{a}} \\ v_{\mathrm{b}} \\ v_{\mathrm{c}} \end{bmatrix} = \begin{bmatrix} cos(\theta) & -sin(\theta) & 1 \\ cos(\theta - 2\pi/3) & -sin(\theta - 2\pi/3) & 1 \\ cos(\theta + 2\pi/3) & -sin(\theta + 2\pi/3) & 1 \end{bmatrix}\begin{bmatrix} v_{\mathrm{d}} \\ v_{\mathrm{q}} \\ v_0 \end{bmatrix} \quad (14)$$

where, v_{a}, v_{b} and v_{c} are the reference voltages in three phase system. These three-phase voltages are then compared with a high-frequency triangular carrier waveform to generate the pulse signals for each inverter switch, which can control the inverter switches. This method is known as Pulse Width Modulation (PWM). PWM is a method of converting an analog reference signal (such as the three-phase voltages) into a digital signal (0 or 1). Here, the frequency of the triangular wave carrier equal to the switching frequency is set to 10 kHz. The three signals generated in this method with their NOT-signals are the PWM signals applied to the inverter switches Q1 – Q6.

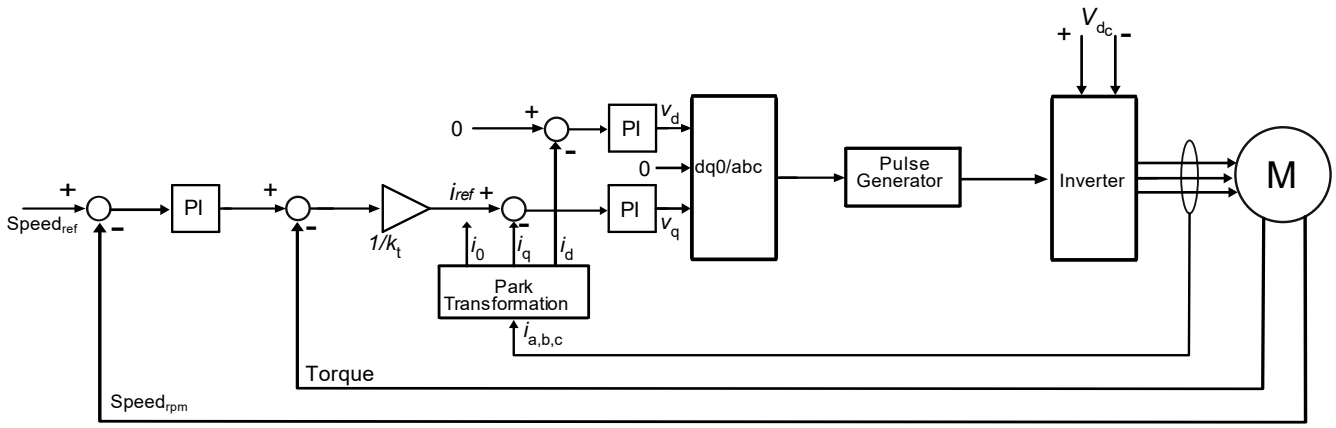

FIGURE 5: BLOCK DIAGRAM OF CCFOC-BASED CLOSED-LOOP SPEED AND TORQUE CONTROL FOR A BLDC MOTOR.

III. RESULTS AND DISCUSSION

The introduced control methods were simulated in the MATLAB/Simulink environment for controlling a 350 W BLDC motor of an e-scooter over a period of 0.3 s. The simulation results for comparing the speed and the torque diagrams are illustrated in FIGURES 6 and 7, respectively. Initially, as shown in FIGURE 6, the reference speed was set to 418 rpm, corresponding 20 km/h based on a 10-inch wheel diameter of the e-scooter, and the load torque was maintained at 1.5 Nm. To evaluate the model's sensitivity to speed and load changes, the reference speed and load were reduced to 315 rpm at $t = 0.12$ s and the mechanical load was increased to 2.2 Nm at $t = 0.15$ s. Additional changes in the reference speed and the mechanical load were conducted at $t = 0.16$ s, $t = 0.2$ s, $t = 0.22$ s, and $t = 0.25$ s, as shown in FIGURES 6 and 7.

From FIGURE 6, the CC-FOC control method was able to stabilize the motor speed at the reference speed of 418 rpm in 0.04 s, but the HSC control method required more than 0.12 s. After the speed reduction at t=0.12 s, t=0.16 s and t=0.22 s, both control systems responded effectively, stabilizing the motor speed at the new reference value in less than 0.01 s. These indicate that the CC-FOC method has a significantly higher response capability at maximum speeds compared to the HSC method.

It can be seen from FIGURE 7 that at high loads, the torque ripple in the CC-FOC control method is significantly less than the torque ripple in the HSC control method. With the load reduction and the motor speed reduction from 0.2 s onwards, the torque ripple in the HSC method gradually decreased. This shows that the CC-FOC method can control the motor much better and more smoothly at high loads compared to the HSC method.

In CC-FOC method, by increasing the load, no visible change occurred in the speed diagrams, indicating that the motor successfully maintained its speed without ripple. In HSC method, the torque diagram shows that both speed and load variations proportionally affect the motor's torque ripple. As a result, the CC-FOC method reduces torque ripples and improves the dynamic stability of the system.

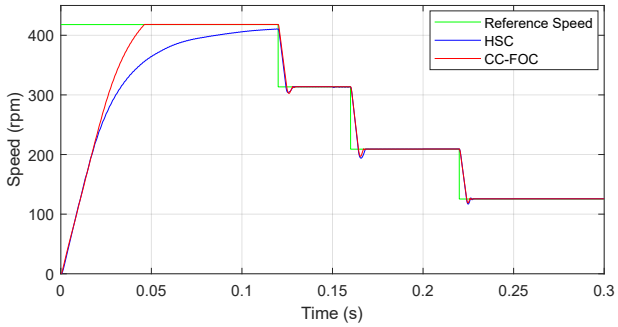

FIGURE 6:BLDC MOTOR SPEED COMPARISON BETWEEN CCFOC AND HSC CONTROL STRATEGIES.

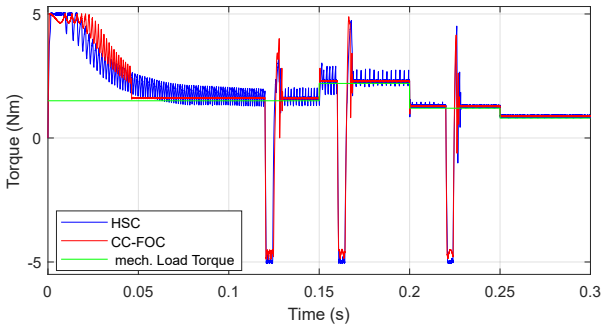

FIGURE 7:BLDC MOTOR TORQUE COMPARISON BETWEEN CCFOC AND HSC CONTROL STRATEGIES.

IV. CONCLUSION

This paper investigated the effect of two different control methods, CC-FOC and HSC, on the speed and torque control of BLDC motors. Simulation models are developed in MATLAB/Simulink environment to evaluate each technique under identical operating conditions for a 350-W BLDC motor used in an electric scooter. The findings show that CC-FOC method significantly reduces torque ripple and improves the dynamic stability of the system compared to the HSC method. These results indicate that CC-FOC provides superior control precision, making it more suitable for not only high-performance electric vehicle applications, but also for drones, and robotics applications where smooth torque, efficient operation and fast dynamic response are essential. On the other hand, the HSC method remains a practical and cost-effective option for low- to medium-performance systems, such as small electric scooters, fans, and household appliances, where

simplicity, robustness, and reduced control hardware requirements are more important than fine torque regulation.

Future research could focus on combining both control strategies in an adaptive framework that switches between them based on load, speed, and efficiency demands to achieve an optimal trade-off between performance and system complexity.

REFERENCES

[1] A. Basarur, J. Mayer, A. Zea and U. D. Hanebeck, “Position and Speed Estimation for BLDC Motors Using Fourier-Series Regression”, IEEE 23rd International Conference on Information Fusion, 2020.

[2] I. M. Alsofyani and N.R.N. Idris, "A review on sensorless techniques for sustainable reliablity and efficient variable frequency drives of induction motors", Renewable and Sustainable Energy Reviews, Elsevier, 2013.

[3] P. Singh and P. Gaur, "Grid interfaced solar water pumping system with improved space vector modulated direct torque control", Ain Shams Engineering Journal 11, Elsevier, 2020.

[4] M. Hussein, M. E. Shalaby, H.A.M. Shatla and A. Refky, "Speed Control of a Three Phase Induction Motor Using Field Oriented Control", JMEST, 2015.

[5] M. N. Gujjar and P. Kumar, "Comparative analysis of field-oriented control of BLDC motor using SPWM and SVPWM techniques", IEEE International Conference on Recent Trends in Electronics Information & Communication Technology (RTEICT), 2017.

[6] D. Mohanraj, R. Aruldavid, R. Verma, K. Sathyasekar, A. B. Barnawi, B. Chokkalingam and L. Mihet-Popa, "A Review of BLDC Motor: State of Art, Advanced Control Techniques, and Applications", IEEE 2022.

[7] S. Singh, N. B. Y. Gorla, K. Jayaraman and J. Pou, “Analysis and mitigation of common-mode noise with different modulation strategies in SiC-fed three-phase brushless DC motor drive”, IEEE JOURNAL OF EMERGING AND SELECTED TOPICS IN POWER ELECTRONICS, 2024.

[8] R. Bhosale, W. Warshe, M. P. Shreelakshmi, P. Arlikar, A. K. Prakash and V. Agarwal, “Performance comparison of Two PWM techniques applied to BLDC motor”, 2018 International Conference on Power, Instrumentation, Control and Computing (PICC), 2018.

[9] V. K.R. Singh Patel, A.K. Pandey, “Modeling and Performance Analysis of PID Controlled BLDC Motor and Different Schemes of PWM Controlled BLDC Motor”, IJSRP, 2013.

[10] R. Lajić and P. Matić, "Digital Position Control System with a BLDC Motor Using Field Oriented Control", 22nd INFOTEH, East Sarajevo, Bosnia and Herzegovina, 2023.

[11] C. J. O’Rourke, M. M. Qasim, M. R. Overlin and J. L. Kirtley, "A Geometric Interpretation of Reference Frames and Transformations: dq0, Clarke, and Park", IEEE Transactions on Energy Conversion, 2019

[12] S. Solgi, A. Stadler, K. Pourhossein, A. Jahic, M. Plenz and D. Schulz, "Modeling, Simulation, and Performance Evaluation of a Commercial Electric Scooter", World Electric Vehicle Journal, 2025.